MS.ID-IJPBS-2679
International Journal of Pharmacy and Biological Sciences-IJPBS™ (2025) 15 (1): 53-67
Online ISSN: 2230-7605, Print ISSN: 2321-3272
Research Article | Pharmaceutical Sciences | OA Journal | MCI Approved | Index Copernicus

Design, Formulation and Evaluation of Enzalutamide Nano Sponge Using BOX-Behnken Design for Management of Prostate Cancer

Srinivas Pooduri*[1], Seema Tomar[2] and M. Srinivas Reddy[3]

***[1]Research Scholar, Faculty of Pharmaceutical Sciences, Motherhood University, Dehradun Road, Karoundi village, Bhagwanpur post, Roorkee Tehsil, Haridwar Distt., Uttarakhand, India-247661.**

[2]Professor, Faculty of Pharmaceutical Sciences, Motherhood University, Dehradun Road, Karoundi village, Bhagwanpur post, Roorkee Tehsil, Haridwar Distt., Uttarakhand, India-247661.

[3]Professor, Beside L.M.D Police Station, Ramakrishna Colony, Thimmapur, Karimnagar, Telangana State, India-505527

Received: 12 Nov 2024/Accepted: 20 Dec 2024/Published online: 01 Jan 2025
***Corresponding Author Email:** srinuvas004@gmail.com

Abstract

Enzalutamide (EZL) is a potent androgen receptor inhibitor widely used for the treatment of metastatic castration-resistant prostate cancer (mCRPC). However, its poor aqueous solubility and limited oral bioavailability pose significant challenges in achieving optimal therapeutic outcomes. This study aimed to design and evaluate a sustained-release nano sponge (NS) delivery system for EZL using β-cyclodextrin (β-CD) as the polymer matrix. Nano sponges were prepared by the solvent evaporation method using dimethyl carbonate as a cross-linker and optimized through a Box-Behnken Design (BBD) under a Quality by Design (QbD) framework. The effects of polymer concentration, cross-linker amount, and reaction time were assessed on critical quality attributes such as particle size, entrapment efficiency, polydispersity index (PDI), and zeta potential. The optimized formulation exhibited a particle size of 168.9 nm, entrapment efficiency of 85.47%, and zeta potential of −26.75 mV, indicating good colloidal stability. Characterization through FTIR, DSC, and XRD confirmed successful drug encapsulation and reduced crystallinity. In vitro drug release studies demonstrated a biphasic release profile with sustained drug release up to 88.5% over 12 hours. Furthermore, pharmacokinetic evaluation in rats revealed a 2.5-fold increase in bioavailability, extended half-life, and improved mean residence time compared to free EZL. The findings suggest that β-CD-based nano sponges are a promising nanocarrier system for enhancing the solubility, stability, and therapeutic performance of EZL. This approach may improve patient compliance and treatment efficacy in prostate cancer therapy.

Keywords

Enzalutamide; Box-Behnken Design; prostate cancer; β-cyclodextrin; Pharmacokinetic; Nano sponges.

*****

INTRODUCTION

Enzalutamide (EZL) is a novel androgen receptor inhibitor that has revolutionized the treatment of advanced metastatic Castration-Resistant Prostate Cancer (mCRPC) [1]. Its mechanism of action, targeting the androgen receptor signaling pathway, has proven to be an effective strategy against prostate cancer growth [2, 3]. EZL belongs to Bio pharmaceutics Classification System (BCS) Class II, exhibits relatively low aqueous solubility, presenting a challenge in developing oral dosage forms. Its limited solubility may result in poor bioavailability, affecting drug absorption and systemic exposure [4, 5].

All cancers in general, prostate cancer is the second most frequent in males and the fifth leading cause of cancer-related deaths globally. Treatment options for primary or localized prostate cancer are mostly determined by factors such as the patient's age, biomarker levels, clinical tumor stage, and Gleason score. Even in late stages, the gold standard for treating primary and localized prostate cancer is androgen deprivation therapy, radical prostatectomy, and radiation. Unfortunately, there is currently no way to lessen the side effects of these treatments, and they just increase survival rates for individuals with advanced stages. Impotence and urine incontinence are side effects of radiation therapy and radical prostatectomy, respectively. Radiation therapy also increases the risk of permanent infertility. However, serious adverse effects such diabetes, insulin resistance, erectile dysfunction, bone loss, and lack of interest in sexual activity are associated with androgen deprivation therapy [6]. There is an immediate need to create effective, targeted, and individualized treatment plans because conventional medicine can cause serious side effects and even drug resistance. Here, methods based on nanomedicine show a lot of promise for offering fresh options [7]. When looking at the development of drug delivery systems, nanostructured drug carriers are seen as a potent tool. Because of their distinct physical and chemical characteristics, nanocarriers have attracted a lot of attention from researchers looking into cancer treatment [8]. Their function in lowering the encapsulated drug's negative effects and keeping it from degradation, as well as in facilitating its regulated or sustained release, is now the most crucial hypothesis to be investigated. To further enhance their therapeutic efficiency in vitro and in vivo, it is crucial to comprehend the influence of their properties such surface chemistry, shape, and particle size. A new class of drug carriers with improved selectivity and specificity for malignant tissues has emerged in recent years, made possible by improvements in the control of these key characteristics.

The stability of β-Cyclodextrin Nano Sponges (β-CDNSs) is noteworthy, as they exhibit exceptional resistance to elevated temperatures, withstanding temperatures as high as 300°C. Furthermore, these CDNSs exhibit stability over a broad pH spectrum, ranging from 1 to 11. The fabrication of these nano sponges can be achieved through various techniques, including thermal desorption and ultrasound methods [9]. The preparation of Cyclodextrin Nano sponges (CDNSs) of EZL offers several pharmaceutical advantages. CDNSs can enhance EZL solubility and stability, leading to improved bioavailability and prolonged shelf life. They also allow for Sustained drug release, potentially reducing dosing frequency and improving patient compliance. CDNSs can be functionalized for targeted drug delivery, minimizing off-target effects and improving drug accumulation at specific sites. Furthermore, the adaptability of CDNS formulations offers a number of potential drug delivery system alternatives and suggests that CDNSs may improve the therapeutic efficacy of EZL in treating metastatic prostate cancer and overcoming drug resistance.

Due to the benefits presented by cyclodextrin nano sponges and recognizing the limitations of EZL, our team undertook efforts to develop EZL-loaded nano sponges. We aimed to optimize the EZL-loaded nano sponges utilizing Quality by Design (QbD) principles to ensure an efficient and effective formulation.

MATERIALS AND METHODS:

EZL were obtained as gift samples from Hetero Pvt. Ltd., Hyderabad, India, and were used without further purification. Hydroxypropyl β-cyclodextrin (HP-β-CD) and β-cyclodextrin (β-CD) were procured from Hi Media Laboratories Pvt. Ltd., Mumbai. Ethyl cellulose and polyvinyl alcohol (PVA) were purchased from Loba Chemie Pvt. Ltd., Mumbai. Analytical reagent (AR) grade solvents including dichloromethane, methanol, and ethanol were obtained from Loba Chemie Pvt. Ltd. and Merck Pvt. Ltd., Mumbai. Sodium hydroxide and hydrochloric acid of AR grade were supplied by Hi Media Laboratories Pvt. Ltd., Mumbai. Phosphate buffers were prepared using sodium dihydrogen orthophosphate (Hi Media Laboratories Pvt. Ltd., Mumbai) and potassium dihydrogen phosphate (Lab India, Mumbai). Carbopol 934 and triethanolamine were purchased from Meher Chemie, Mumbai. Surfactants including Tween 80 and Span 60 were

obtained from M/s Alkem Laboratories Pvt. Ltd., Mumbai. A dialysis membrane (MWCO suitable for in vitro drug release studies) was procured from Hi Media Laboratories Pvt. Ltd., Mumbai. All other chemicals and reagents used were of analytical grade and used as received.

Development, Characterization of EZL-NS

Optimization of EZL-NS

A lot of work went into creating best NS for quality goal product profile Very important for product practicality. Therefore, it is an important step that must be highlighted for the end product to be believed to be safe, effective, and of high quality. Nevertheless, this cannot be achieved without giving careful thought to the CPPs and CMAs, which have the potential to influence the CQAs (critical quality attributes) [10]. Table 1 displays all of the QTPP's required components along with their validation for EZL-NS fabrication. Addressing the specific research goals of these QTPPs is crucial. Think about how you'll be using the product; its properties that are relevant to the skin should be perfect for that task. Ishikawa plot (Figure 1) provides more details regarding the development process's risks, necessary conditions, and CQA.

Table 1: QTPP & its rationale for making EZL loaded NS.

QTTP	Target	Justification
Drug Delivery system	Nano sponges	Compared to other nanosystems, it has improved oral retention.
Type of Dosage	Controlled Release	It improves drug absorption.
Administration route	Oral	Non-invasive, on-site medication administration and simplicity of use are their advantages.
Drug release studies (%)	More than 85 %	Optimization of therapeutic and pharmacological action requires it.

β-CD NS Synthesis

Created a CD-based NS utilizing HP-ᵝ-CD and ᵝ-CD polymers, CDI, and dimethyl carbonate as cross-linking agents. Swaminathan et al. (22) has developed hot melt NS using varied polymer-crosslinker molar ratios. To summarize, the anhydrous polymer and the cross linker were combined for several hours at temperatures approximately 90°C. Filtration was used to remove the solid byproduct from the reaction mixture after cooling. The next step was a light grinding to crumble the solid. To remove impurities and unreacted crosslinkers, we conducted a Soxhlet assembled extraction in ethanol. The NS was purified after the reaction with an excess of cross-linker and stored at 25°C until needed again [11, 12].

NS drug loading

Over the course of 24 hours, we meticulously measured drug doses and magnetically stirred NS suspensions in water. Ten minutes at 2000 rpm removed colloidal supernatant from uncomplexed medication. Make antibiotic-loaded NS by freeze-drying colloidal supernatants in a Modulyo (Edwards, UK) freeze dryer. Room-temperature covered vacuum desiccator stored NS for future investigation [13-15].

Fabrication of β-CD-NS

Various excipient amounts, such as β-CD (mol), cross linker concentration (mol), and reaction time (h), were utilized in the emulsion diffusion method to create the NS. The continuous phase contained an adjustable surfactant concentration in a 20 mL water-based cross linker solution, while the dispersed phase contained a 2 mL dichloromethane solution containing the optimal volume of polymer and both medications. Using the specified parameters (35 °C, 1000 rpm for 2 hours), the organic and water phases were mixed. After the NS was collected, there was a drying period of 24 hours at 40 °C [16].

A response surface model is shown using Design Expert®'s integrated data. Incomplete factorial algorithms with three levels produce BBDs of second order (242). Improved NS synthesis was seen in the Box Behnken three-tiered study. Split into two flat parts and a single zero-set part. Using Stat-Ease Inc.'s Design Expert® (12.0.3.0, Minneapolis, MN, USA), we evaluated the second-order algebraic model's quadratic response surfaces. This optimization of BBD requires fifteen trials with three centers. Implicit models are described by quadratic equations, which include the following: duration of reaction (h), concentration of cross linker (mol), and concentration of polymer. Size of particles (Y1), EE, zeta strength (Y4), PDI (Y3), and optimization were affected [17-21]. Table 2 compares the variable to the projected outcomes. Table 2 contains all of the

components, both independent and dependent. Independent factors contribute to the additional data set. The model was defined by seventeen trials with three experimental levels and three factors altogether. Here are the outcomes.

We may summarize the variables the sequence b0, b1x1, b2x2, b3x3, b4x4, b12x1x2, b13x1x3, b23x2x3, b11x21, b22x22, and b33x23 are all integers.

Y represents the coded independent variables X1, X2, and X3, B0 is the intercept, and X2 is the measured response for each component match. Get the b1-b33 regression coefficients from experimental Y-values. The interaction and quadratic terms are XiXj because i and j might be 1, 2, or 3 [22, 23]. Based on the low (−1), medium (0), and high (+1) values from the experiment, choose the polymer molar concentrations (X1), cross linker concentrations (X2), and reaction time (X3). Three variables were measured: particle diameter, entrapment effectiveness, and profile depth index.

Table 2: Box-Behnken Design dependent as well as independent factors including levels and objectives

Parameter	Low (-1)	Medium (0)	High (+1)
Independent Variables			
A: Polymer concentration (mol)	1	2	3
B: Cross linker concentration (mol)	1	5.5	10
C: Reaction time (h)	1	2	3
Dependent variables			
Y1: Particle size (nm)	Minimize		
Y2: Polydispersity index	In range		
Y3: Entrapment efficiency	Maximize		

Based on the results, BBD is clearly the superior experimental design. All signs point to less work and time spent with three variables, twelve runs, and three center-point replicates. The analysis makes use of three main levels of coding for each component. To avoid potentially undesirable outcomes, experiments conducted under extremely high or low conditions are irrelevant [24, 25]. Based on Table 13, we can deduce the dependent and independent variables

Checkpoint Analysis

By solving the related polynomial equations, we were able to discover the theoretical values of PDI, zeta potential, particle size, and entrapment efficiency. We took three points at random from each contour plot and used them as a control variable. At each of the three checkpoints, the theoretically obtained values were compared statistically to those of the experimentally prepared nano sponge formulation [26].

We used multicriteria decision analysis (MCDA) to combine the two responses into a single composite response system, optimizing the NS entrapment efficiency and particle size simultaneously. To compensate for the drawbacks of unstructured decision-making, MCDA offers a methodical approach to selecting options using multiple criteria [27]. By utilizing the desirability function in Design-Expert® Version 9.0.6, the ideal NS formulation was derived. We can forecast the ideal point that stands for maximum desirability with the use of software optimization tools and the desirability criteria of response surface methodology. These tools identify which variables had an effect on each response and how large that effect was. The nature of the objective might change depending on how the points are weighted for each answer. The goal fields for each answer can take on one of five possible values: inside range, target, minimum, maximum, or none. Here is the next logical step after numerical optimization: graphical optimization. The factors' relationships with the response could be examined more thoroughly using overlay and desirability plots. In order to find the best formula, two parameters were considered: maximum entrapment and ideal particle size [28].

Formulation Optimization

Moreover, response surface plots [29] graphically demonstrated the impact of each variable on the responses. The software's overlay plot then used the specified goals and constraints to foretell the optimal nano sponge formulation formulas. Additional validation of the optimized formulae with desirability factors close to one was achieved by the use of a comparison between the software's projected response values and those produced experimentally.

Characterization of Prepared β-CD-NS

The optimized NS was characterized using a number of different processes. We used SEM, TEM, DSC, and XRPD. Productivity, particle size, entrapment, zinc potential, and PDI were among the other parameters assessed [30].

Particle characterization

UK-based Malvern Zetasizer Nano ZS measured particles. Polystyrene cuvettes held 1:200 distilled water-diluted inquiry samples. We measured particle size and PDI using DLS. A cuvette was used to assess zeta potential and all other potentials. Every one of the three samples was examined three times [31].

Efficiency of entrapment (EE) along with drug loading

The dispersion filtrate was tested for drug loading (DL) and the efficiency of entrapment (EE) after 30 minutes of ultracentrifugation at 16,900 xg and 4 0C. For this purpose, we utilized the 5418R centrifuge, which is made by Eppendorf of Hamburg, Germany. The concentrations of EZL were measured using UV-visible spectroscopy at 234 and 270 nm [32], after filtering the supernatant. To calculate the EE and DL of EZL loaded NS, we employed the following equations [33].

Entrapment efficiency (%) = (Initial amount of drug added-Drug amount in supernatant)/ (Initial amount of drug added)

Drug loading (%) = (Initial amount of drug added-Drug amount in supernatant)/(Total amount weight of nano sponge)

Size of the particles, PDI, potential of Zeta

In order to determine the zeta potential, particle size, and PDI of nano sponges, a Malvern Zetasizer (nano ZS, Malvern instruments Ltd., UK) used dynamic light scattering. To ensure accurate results, we used a clear, disposable zeta cell to thoroughly mix the samples with double distilled water before examination. To reduce the margin of error, we examined each sample three times and maintained the instrument temperature at 25 °C throughout [34].

Solid State Properties

Infrared Fourier transform

A range in substances was examined by taking and analyzing FTIR spectra; these included optimized EZL and pure EZL. Finding potential chemical interactions was the aim. To ensure the medication was compatible with the formulation's excipients, a custom-built Shimadzu FTIR spectrophotometer was employed. This study employed a pellet technique involving potassium bromide (KBr). Upon careful mixing, a solution of dried potassium bromide crystals was introduced to the samples. A squeeze was applied to the mixture. The range of 400 to 4,000 cm−1 was captured by using the sample cell's disk to gather spectra. In order to compare the two versions of the natural medicine, we obtained their FTIR spectra [35].

Differential scanning Calorimetry analysis (DSC)

All sorts of compounds, including pure EZL and optimized EZL, were observed using a DSC system it runs on nitrogen and aluminum 10-300°C/min. The experiment employed nitrogen for purging. This took place in non-hermetic aluminum pans. It was only after precise measurement that the powder samples were placed in the pan and covered with the lid. We utilized a sealed, empty pan as a point of reference. After that, thermograms were taken by placing the pans on the instrument's auto-sampler tray [36].

X-ray diffraction studies (XRD)

A combination of an auto sampler and an X-ray diffractometer operating at 40 kV/20 mA was used to record an XRD pattern of the prepared nano sponges. The samples were scanned using a continuous scanning type setup with a k-beta filter at 3 and 50 degrees 2. To ensure the medication had been enclosed, we looked for shifts in unique peaks that did not conform to the usual drug spectrum [37].

***In Vitro* Release Studies**

Activated dialysis bags in a dissolving chamber were used to study DS, EZL-NS, and commercial EZL medication release. A system speed of 100 rpm and an operating temperature of 37 ± 0.5 °C were involved. For this purpose, we devised phosphate buffers with physiological pH 7.4 and intestinal pH 1.2. This allowed us to ascertain the release profile. If you want to keep the sink state going, just add 5 mL of new dissolving media to the reservoir every time. Purified and quantified at 210 nm. Applying many kinetic models to the data allowed us to determine the drug release mechanisms and their kinetics [38, 39].

***In vivo* Pharmacokinetic Studies**

The pharmacokinetic study divided six male Sprague Dawley rats (n=6) into three groups at 8-10 weeks. In a specific order, the third group got EZL and at mg/kg BW intravenously (iv). First and second groups received oral EZL-NS and free-EZL solutions. With LAC-2017-0282, Motherhood University met its requirements. After treatment, half a milliliter of blood was drawn at 5, 10, 45, 60, 120, 240, 480, 720, and 960 minutes. Blood samples were taken by spinning heparinization tubes at Rotate at 4000 rpm for 10 minutes at 4 °Cr. The liquid beyond the solid phase was frozen at -80 °C. Was HPLC-UV analyzed? Protocol for detecting in rat plasma: Using this approach, a column thermostat at 30 °C, 5 µL sample injection, and 0.8 mL/min HPLC-UV at 268 nm were used. Considerations for this investigation included: 0.1 M acetate buffer and 10:1 methanol formed the mobile phase. Five µL of hydrochloric acid were added to two liters of 16.4-gram sodium acetate buffer to correct the pH to 5.0. The PK parameters,

including mean ± SD values for each treatment group, were analyzed non-compartmentally. Calculated and displayed using standard deviations: When analyzing the plasma drug concentration-time curve, the important variables to consider are the terminal elimination rate steady state (Ke), half-life (T1/2), AUC0-last, and AUC0→∝ [40].

Analysis of statistical Data

Unless otherwise specified, reports are shown as the average augmented or diminished by the dispersion of the data significance level in one-way analyses of variance or p-values below 0.01, which signified the t-tests.

RESULTS AND DISCUSSION

Synthesis of CD NS

First, CD-based NS is made by carefully crosslinking the polymer with the cross linker. Then, the NS is refined to remove any chemical impurities and unreacted cross linker. Finally, the drug is loaded into the blank NS. The polymer employed in this study was DMC was used as the cross linker for HP-β-appropriate proportions of cross linker to polymer critical variable in NS synthesis. An ideal crosslinking strength between CD molecules would be somewhere in the middle, allowing for the construction of stable nano scale NS. More drugs than NS produce drug: CD complexes. This final complex will have low drug inclusion & non-inclusion complexation. Conversely, an excessively high degree of crosslinking causes NS to lack drug molecule binding sites when the cross-linker concentration is too high in comparison to the polymer. Therefore, it is expected that an optimal balance of the two would be attained for the finest NS with the greatest drug entrapment and other viable attributes. After looking over the relevant literature, doing trial and error experiments, and thinking about the fundamental facts, the polymer to cross linker ratios were determined. Statistical validation and optimization of the same were also achieved by combining the QbD approach with Box Behnken Design (BBD). The procedures outlined in the methodology part were used to create the NS; these techniques are derived on the classic hot melt method first detailed [45].

Table 3: Design of EZL Nano sponge using BOX-Behnken

Std	Run	A	B	C	Y1	Y2	Y3	Y4
1	8	1	1	2	342.15±2.35	0.458±0.02	69.85±0.35	-20.35±0.12
2	13	3	1	2	296.88±3.14	0.239±0.04	75.42±0.42	-34.51±0.35
3	11	1	10	2	461.23±2.03	0.358±0.01	67.31±0.15	-40.28±0.24
4	6	3	10	2	235.68±1.36	0.428±0.03	69.28±0.16	-32.61±0.13
5	12	1	5.5	1	362.59±3.25	0.284±0.11	75.13±0.85	-24.19±0.16
6	2	3	5.5	1	168.92±1.46	0.132±0.12	85.47±0.34	-26.75±0.28
7	16	1	5.5	3	339.65±2.05	0.306±0.15	72.31±0.25	-30.62±0.35
8	4	3	5.5	3	250.13±1.26	0.246±0.06	70.53±0.16	-27.46±0.27
9	7	2	1	1	196.84±3.24	0.192±0.08	73.62±0.22	-30.27±0.18
10	15	2	10	1	273.69±1.25	0.273±0.03	77.48±0.14	-38.96±0.15
11	5	2	1	3	260.51±2.16	0.276±0.03	76.09±0.17	-34.15±0.18
12	14	2	10	3	315.24±2.34	0.312±0.05	67.31±0.18	-39.86±0.19
13	1	2	5.5	2	382.64±3.15	0.342±0.09	48.39±0.16	-22.59±0.36
14	17	2	5.5	2	389.46±3.62	0.359±0.04	46.13±0.18	-24.51±0.24
15	10	2	5.5	2	380.16±2.15	0.355±0.06	45.78±0.14	-20.61±0.15
16	9	2	5.5	2	365.74±2.18	0.349±0.04	43.12±0.32	-24.19±0.39
17	3	2	5.5	2	370.42±2.19	0.347±0.07	46.92±0.29	-20.15±0.51

EZL-NS characterization, optimization

i. size of the particle (R1), measurement in Zeta potential

The size of the EZL-NS particles is an important performance component since it determines the amount and pace of drug release, and hence its absorption. The greater surface area available for diffusion in smaller particles enhances drug release. All scheduled trial runs' particle sizes were checked by DLS. We used software to study numbers and graphs. All about R1 and A, B, and C the best-fitting mathematical model yielded the following equation: The particle size is the result of multiplying the following variables: The formula is: +377.68 -69.25A +23.68B +20.44C -45.07AB +26.04AC -5.53BC -12.47A2 -31.23B2 -84.89C. ^2. Predicting the proportionate influence of variables on response R1 was also made possible by using different graphs. Plots of the 3D reaction surfaces and contours for different component combinations that impact the response particle size (R1). According to the polynomial equation and graphs, the polymer

concentration directly and positively affected particle size (R1), but the cross-linker concentration had no influence [46].

The difficulty of visualizing the response surface using graphical tools increases with the number of RSM components. In these cases, "perturbation" and "interaction" response graphs are necessary for displaying RSM data. A perturbation plot parameter with a sharply sloping curve, which examines the influence of all components at one point in RSM design space, indicates a relatively high level of response sensitivity. But if everything else stays the same, you may use an interaction plot to see how different independent variables affect each other. Figure 21 displays the particle size (R1) cube graphs in addition to the expected vs. actual, perturbation, and factors interaction graphs. The expected vs. reality plot showed a better degree of linearity in all the trial run formulations. The change from -1 to +1 for variables A and B significantly enhanced reaction R1. R1 was somewhat enhanced by factor C. In addition, the results from the polynomial equations matched up with the interaction plots, which showed how the solution was impacted by the combined independent components. There was more proof that different factor combinations affect particle size from this [47].

The average particle size went from 168.92±1.46 to 461.23±2.03 nm when the polymer concentration was raised from 1 to 3 (mol). Perhaps the larger NS particles are a result of the crosslinking aggregates formed at greater concentrations by the mixed polymeric matrix. Without the proper quantity of cross linkers, CD complexes containing medicines instead of NS (small or big in size) may also form at very high polymer concentrations. Crosslinking becomes easier and bigger cross linked polymeric agglomerates are produced more quickly as the cross-linker content in the reaction mixture is increased [48].

The improved EZL-NS's size and distribution pattern were determined using particle size analysis. In Figure 22, we can see the stated size distribution. On average, the optimized EZL-NS had a diameter of 168.92±1.46 nm, a PDI of -26.75±0.28 mV, and a Zeta potential of -26.75±0.28 mV. A multimodal distribution was evident in the examined NS sample due to the high PDI value. This is the result of the DLS method's hydrodynamic size distribution prediction, which is biased toward bigger particles (259,260) in most samples. It is not always easy to manage the size distribution of polymeric NPs, in contrast to nano emulsions and metallic NPs [49]. The carbonate groups in the EZL-NS sample's structure promoted electrostatic repulsion among the NS particles (193), keeping them physically stable by preventing aggregation, which likely led to a sufficiently high Zeta potential. The optimized NS demonstrated the successful tuning of the synthesis process parameters by exhibiting an optimum size and Zeta potential.

Model significance is illustrated by a 54.85 F-value. A high F-value is unlikely to be attributed to chance with 0.01% probability. A p-value of 0.0500 or less indicates model term significance. The A, B, C, AB, AC, B^3, and C© variables serve as main examples of this in the model. Any number over 0.1000 renders the provisions of this model meaningless. A 3.56 F-value indicating no fit on statistically equivalent to an honest error. In 12.59% of cases, noise might be to blame when the lack of Fit rating is high (F-value).

There is a less-than-0.2-point change from the expected R^2 of 0.8313 to the revised R^2 of 0.9680. With Adeq Precision, you can determine the signal-to-noise ratio. A ratio of at least 4 is considered ideal. There is a signal-to-noise ratio of 28.985. With this model, you can circumvent the design space in one shot.

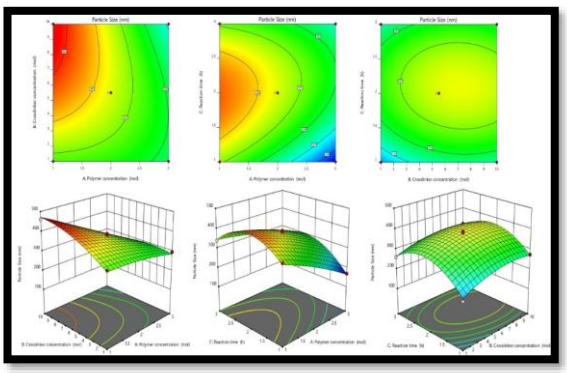

Figure 1: Particle size as a dependent variable with Figure shows how polymer concentration (A), cross linker concentration (B), and reaction time (C) affect this dependent variable in three-dimensional response surfaces and contour plots.

The design reveals a very significant F-value of 101.46. Such a high F-value could only be the result of an extremely minuscule chance (0.01%). With p-values below 0.0500, we may identify important model terms. Crucial to the model's operation are the variables AB, AC, B^3, and C. Any number above 0.1000 indicates that the model terms do not have statistical significance. Improving your model requires you should remove words that aren't essential for hierarchy. Unfitness is likely with an F-value of 4.58 of noise producing an F-value of this magnitude is 8.79%.

Entrapment efficiency

The results for all batches made using BBD are shown in Table, which was constructed after looking at several aspects to see how they affected the entrapment power. R2 improved with polymer (A), cross linker (B), and reaction time (C) adjustments. Depending on the batch that the software suggested, the entrapment efficiency might range from 39% to 81.64%, with the polymer concentration playing a pivotal role. This is the equation that was produced by the best mathematical model: Entrapment Efficiency = +46.07 +2.01A -1.70B -3.18C -0.9000AB -3.03AC -3.16BC +13.32A2 +11.08B2 +16.48C2. As seen in Figure 23, the entrapment efficiency shows a significant increase with increasing polymer concentration. Alternatively, it was shown that increasing the cross-linker concentration improved the medicine's entrapment efficiency in NS by decreasing its capacity to escape into the exterior phase. Shorter reaction times also led to better trapping efficiency.

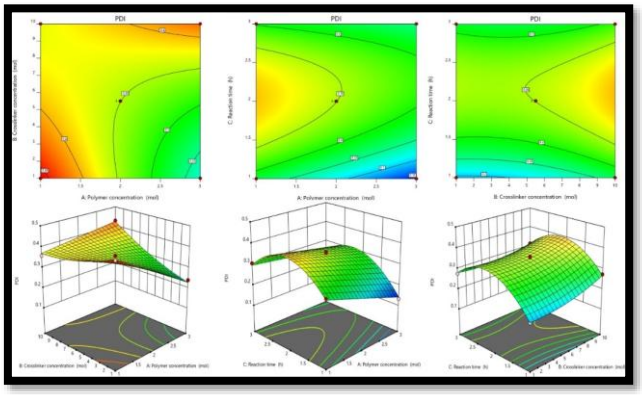

Figure 2: The relative effects of polymer concentration, cross linker concentration, and reaction time on EZL-NS PDI are shown in 3D response surface and contour plots.

There is a discrepancy of less than 0.2 between the predicted 0.9031 as the value and 0.9826 as the updated R^2 value. We make use of Adeq to measure SNR. Try to exceed 4. The SNR is 39.271, which is remarkable [50].

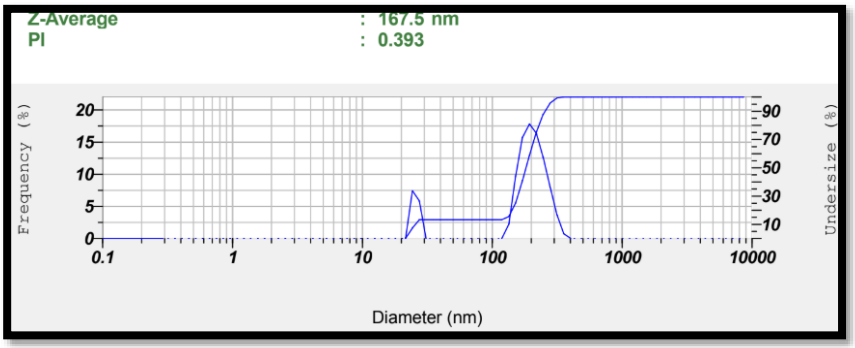

Figure 3: Particle size distribution of the optimized EZL-NS

Assessing and enhancing EZL-NS safety stations

Incomplete factorial designs with three levels were used to produce the rotatable or exceptional rotatable qualities of the second-order BBD design. Based on the results of the three-variable BBD response surface analysis, this research. EZL-NS variables such particle size (nm), entrapment efficacy (%), polymer concentration (mol), cross linker concentration (mol), and reaction time. Quadratic response surfaces are analyzed using second-degree polynomial BBD. Optimizing process variables with little experimental effort is its goal. The available

space for the design was maximized by using two plots: one for the wants and one for the overlays. When applying typical limits such as the optimal particle size (168.92±1.46 & 85.47±0.34) and the maximum entrapment efficiency that could be attained, the best formulation, F6, was found that ideal course of action for determining the variables' optimum concentrations was shown in an overlay plot, as illustrated in Figure. This graph was analyzed using the principle of equilibrium. Another kind of contour plot, an overlay plot provides a visual representation of the design space for inspection. Overlay plots show you where your odds of obtaining the perfect formula that produces the desired results are greatest. You could see the outcomes in a figure that combined the optimized formulation with the determined desirability flag. With respect to the above variables, the optimal values are A=2.968, B=8.024, and C=1.021, where DoEs denote degrees of freedom.

After reviewing the trial's design, we estimated the response value and utilized it to draw a desirability curve. It is feasible to find the best formulation by seeing all potential desire curve independent variable values. After finishing the EZL-NS design space investigation, we generated the best batch or check point and used overlay and desirability plots to assess the accuracy of the design. Before preparing the improved formulation (CN16) for the checkpoint evaluation, we evaluated both responses. Regarding the optimized formulation, the response variables R1, R2, and R3 were 168.92±1.46 nm, 85.47±0.34%, and 0.306±0.15, respectively. Checkpoint analysis allowed us to compare predicted and actual response values, which allowed us to calculate the relative error.

A noteworthy model is one in which the F-value is 76.50. Given the very high F-value, the only plausible explanation is pure chance (with a mere 0.01% probability). Model terms are significant if $p < 0.0500$. This model uses key terms such as A, C, AC, BC, A^2, B^2, and C'. A score over 0.1001 implies non-significant model terms. Considering the substantial inadequate Fit F-value and modest impact size (1.30), the error is easily discernible. An F-value of "Lack of Fit" occurs 38.91% of the time due to noise.

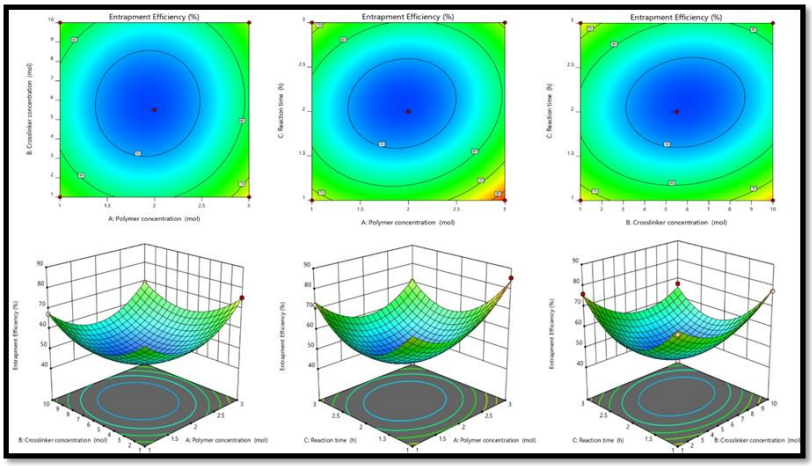

Figure 4: Reaction length, polymer concentration, and cross linker concentration are the independent variables, while the dependent variable is EZL-NS entrapment efficiency.

The connection between these factors is shown visually in three dimensions using contour plots and response surface plots. R^2 prediction of 0.9125 and the Actual R^2 of 0.9770 are within acceptable ranges, since the compare the two with Adeq Precision to determine the signal-to-noise ratio; the discrepancy is less than 0.2. Four is the sweet spot for perfection. Having a ratio of 24.169 indicates a strong signal. Get around the design process more easily using this model.

Table 4: Check point analysis for optimized EZL-NS formulation (F6)

F6	A	B	C	Y1	Y2	Y3	Desirability
Predicted	2.968	8.024	1.021	154.981	86.044	0.216	0.977
Observed	3	5.5	1	168.92±1.46	85.47±0.34	0.132±0.12	
Relative Error	0.032	-2.52	-0.02	13.939	-0.574	-0.084	

iii. FT-IR spectroscopy

Verifying the EZL-NS interaction and trapping inclusions and non-inclusions in NS using FT-IR spectroscopy were followed by F6 optimization of EZL-NS. An interaction between EZL and NS is shown in Figure 27, which exhibits the FT-IR spectrum. These were the peaks seen at 1726-1734 cm−1, 1424-1401 cm−1, and 1027-1030 cm−1. Some EZL peaks were seen at 1090.66, 1028.09, 943.22, 757.57, and 529.48 cm−1. it was shown that EZL and NS interacted. That being said, the EZL is most certainly caught in the NS cage circuit.

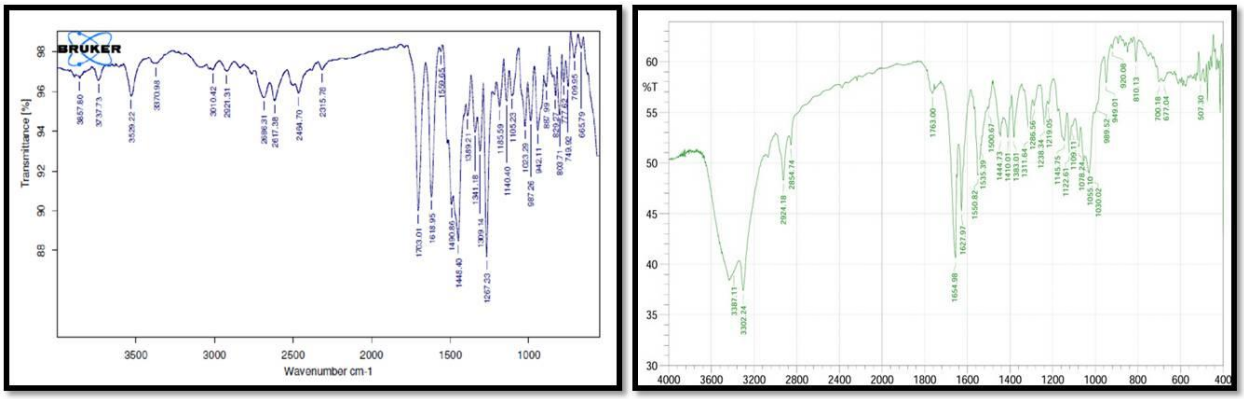

Figure 5: FTIR spectrum of pure drug and optimized EZL-NS

DSC analysis

Using DSC, researchers may study the physical condition of a medication put in NS and examine the thermal behavior of NS—an incredibly useful tool. See Figure 28 for a DSC thermogram of the improved EZL-NS. At 201.62°C, pure EZL melts, DSC analysis showed a decreasing enthalpy with time and an endothermic peak. The endothermic peak of the NS physical mixture thermogram is less visible in Figure 19B than 19A. The melting peak, which is often seen in NS-EZL inclusion, non-inclusion complexes, was absent from an EZL-NS diffractometer. Due to its encapsulation and molecular distribution in NS, the medication was unable to crystallize, therefore there was no DSC signal. This proved EZL and NS interacted. Similar results were observed by Rao et al. (183).

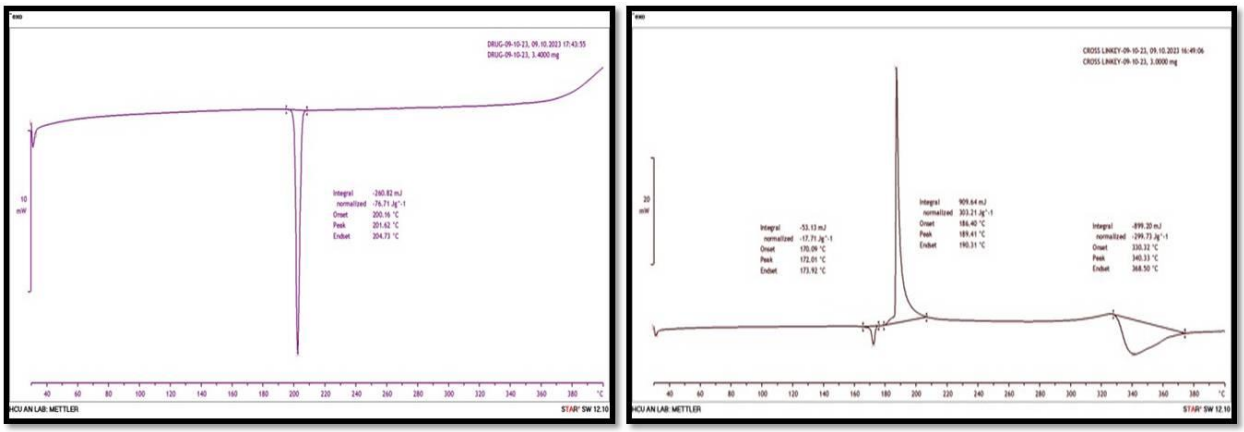

Figure 6: DSC Thermogram of pure drug and optimized EZL-NS

XRPD analysis

It is possible to determine the crystalline state of EZL inside the NS and the way in which we evaluate the interaction utilizing XRPD data from EZL, HP-~-CD, and EZL-NS samples. Shende et al. (186) found that pre-encapsulating HP-β-CD NS results in the medication losing its crystallinity and becoming amorphous. XRPD investigation supported the crystalline structure of pure EZL, revealing peaks at 2θ values of 10.3°, 12.4°, 18.6°, 19.5°, and 20.7° It also had smaller peaks at 14.2°, 16.7°, 18.8°, 19.9°, 24.4°, 27.5°, and 28.2° (251). Wang et al. (262), discovered an HP-β-CD shapeless XRPD pattern.

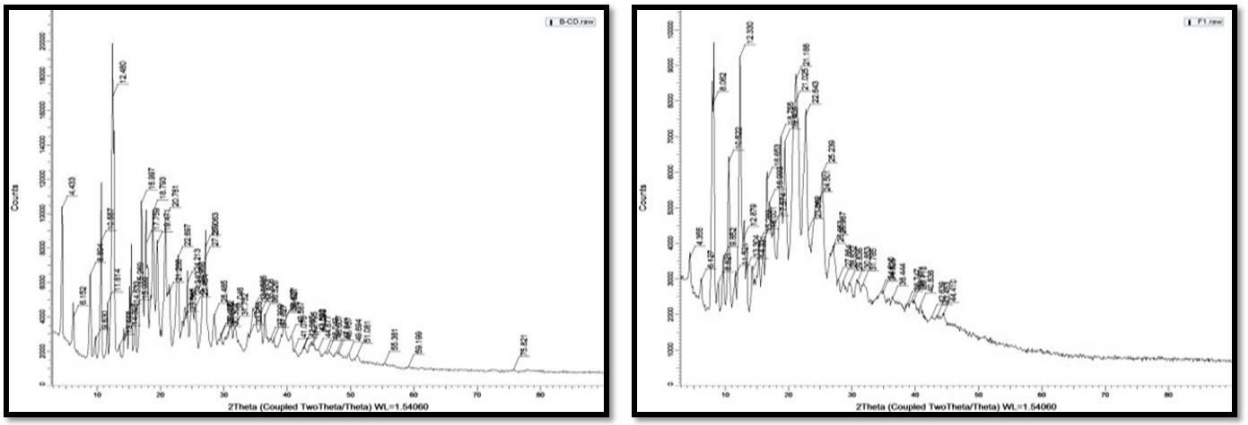

Figure 7: Powdered X-ray diffractogram of pure drug and optimized EZL-NS

A broad peak appears in the absence of diffraction peaks. 20-30° 2θ region confirmed this. Peaks in the NS physical combination match the EZL crystalline structure. Due to HP-β-CD dilution, EZL peaks may be less noticeable here (251). NS made EZL amorphous, creating the XRPD pattern (Figure 29D). of the EZL-NS sample did not exhibit any crystalline peaks. Rao et al. (183) have previously published comparable findings. The results of FT-IR and DSC were supported by these XRPD results, indicating that the drug had other processes than the mechanical interaction of its components to form complexes.

Drug release studies

To estimate the medication's physiological impact, a 6.8-hour dialysis tube operation and two hours of in vitro drug release testing in PBS under physiological conditions (37 °C, pH 1.2) were necessary. Our lab work focused on analyzing the EZL, EZL-solution, and enhanced EZL-NS. Due to EZL and PSAR's acidic pKa value of 2.84, a pH-1.2 PBS buffer was recommended [45]. In contrast to pure medicine and EZL solution, optimum EZL-NS released 88.5% ± 32.5% in 12 hours with improved consistency. While the former exhibited an unsatisfactory release pattern and the latter had an 83.2 ± 15.34% release in 4 hours. See Figure 6A for context. Based on what we know about the polymeric NS so far, it seems to have a two-stage release mechanism: a fast blast followed by a controlled release. Initial burst release is caused by drug adsorption on the polymeric NS surface and internalize at the outer surface. Quick release allows the NS quickly release any drug molecules on or near its surface into the environment. The medicine is then released in two bursts, the first of which is slower and more closely monitored, and the second of which is less so. Drug delivery systems should behave in this way because it allows the therapeutic effect to start functioning sooner and the medication to be supplied more gradually over time, enhancing the length and effectiveness of therapy. In order to tailor medicine delivery systems to individual patients' requirements and achieve the intended therapeutic impact, it is usual practice to alter the biphasic release pattern [75]. Continuous contents discharge may be explained by the existence of polymers in the nanoparticle. R2 = 0.91 implies a significant connection between formulations; EZL-NS provided the most effective sustained release pattern in this case.

Drug release kinetics

Drug release sequences were shown using Higuchi, Korsmeyer-Peppas, zero-order, and first-order kinetic models. R2 determined that the NS drug-releasing model was the most effective. R2 values for each model are in Table 5. In the Higuchi model, diffusion regulated polymeric NS EZL release (R2 = 0.9888). A model's data fit may be assessed using RMSE, BIC, and Akaike. They let us explore multiple models and choose the best data match. Drug release models are evaluated using root-mean-square error. The closer the RMSE is to zero, the more in sync the data and model are. Using AIC and BIC, statistical models may be fitted to datasets. The more parameters a model has, the less fit it has and the more complicated it becomes. The AIC and BIC may be used to evaluate models and determine which one has the greatest fit and parsimony. The goals and circumstances of the study dictate the optimal value of the statistic. The R2 values for EZL-NS were less than 0.9, indicating that the release patterns did not match by first order aa well as Korsmeyer-Peppas models. Table 5 shows that the Zero Order Higuchi models have R2 values greater than 0.90. Our prediction of the drug delivery system's ENZ release mechanism was based on the diffusional constant (n) as input into the Korsmeyer-Peppas equation. Fickian diffusion was assumed for $n < 0.5$, whereas non-Fickian transport was assumed for values of n between 0.5 and 1.0. Medication ENZ

leaves the EZL-NS matrix of NS via Fickian diffusion. [76], [78].

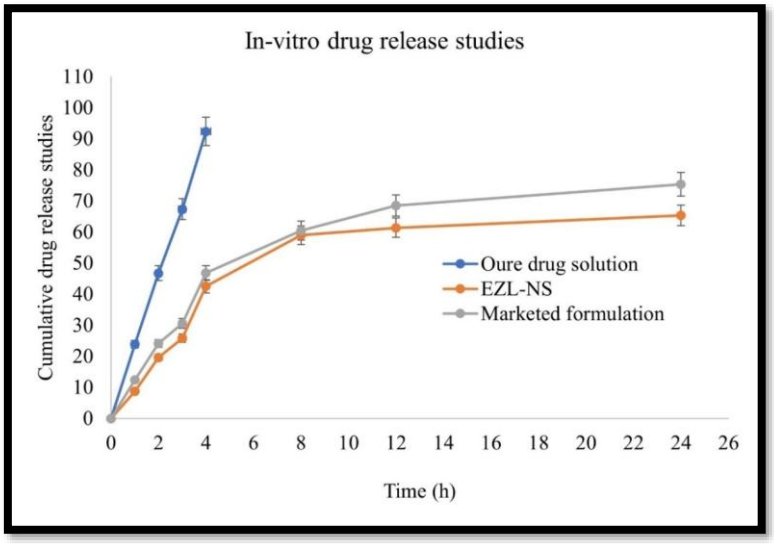

Figure 8: *In Vitro* medication release in optimized EZL-NS along with drug ENZ solution

Pharmacokinetic studies

Several pharmacokinetic parameters were improved in all mouse groups when EZL-NS and EZL solution were given instead of free EZL. AUC, MRT, biological half-life, distribution volume, and starting drug plasma concentration were assessed. After intravenous administration, EZL-NS may boost ENZ medication's systemic availability, half-life, and dispersion due to their strong tissue binding. It may be inferred that EZL-NS may hinder opsonic protein adhesion since its mean residence time (MRT) was significantly greater than that of ENZ alone, at 40.56 ± 6.74. The NS may keep blood circulating for an extended amount of time without being detected by the reticuloendothelial system, as shown in Table 7. This might be the reason the MRT remains for so long. Dunnett's student t-test showed that EZL-NS exhibited significantly higher drug concentrations in plasma, CL, and AUC when contrasted with free EZL. When considered together, these pharmacokinetic features suggest that Treatment effectiveness and medication release duration may be improved by EZL-NS.

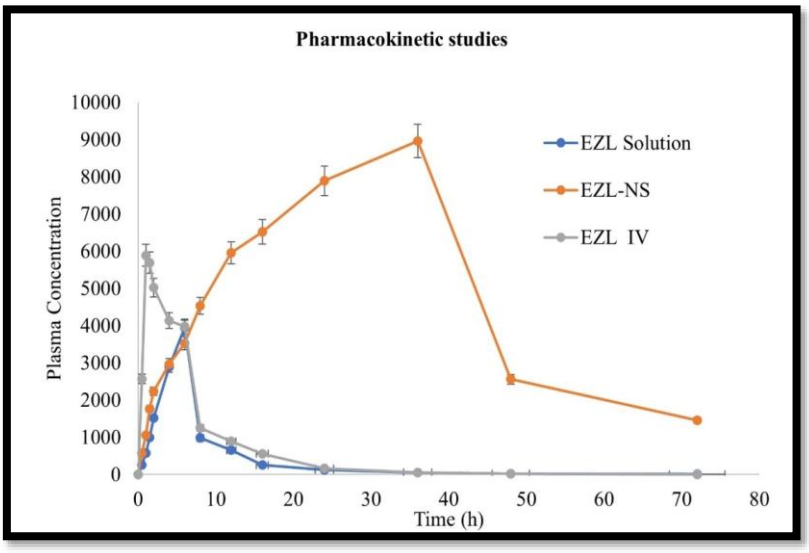

Figure 9: Comparison of Pharmacokinetic studies of optimized EZL-NS and marketed injection

CONCLUSION:

This research focuses on developing a sustained-release drug delivery system for EZL, a key androgen receptor inhibitor used in the treatment of metastatic castration-resistant prostate cancer (mCRPC). Due to EZL's poor water solubility (BCS Class II drug), its bioavailability is limited, making it a suitable candidate for advanced nanocarrier-based systems. To address these challenges, β-cyclodextrin-based nano sponges (β-CD-NS) were prepared using cross-linkers like dimethyl carbonate. The formulation was optimized using Box-Behnken Design (BBD), a statistical approach under the Quality by Design (QbD) framework. The formulation variables included polymer concentration, cross-linker amount, and reaction time, with the responses being particle size, entrapment efficiency (EE), polydispersity index (PDI), and zeta potential. The optimized nano sponge exhibited: Particle size: ~168.9 nm, Entrapment efficiency: ~85.47%, Zeta potential: ~−26.75 mV, PDI: Indicating a moderate size distribution. Characterization techniques like FTIR, DSC, and XRD confirmed successful drug loading and encapsulation, indicating reduced crystallinity of EZL post-formulation. In vitro drug release studies showed a biphasic release profile, with the optimized EZL-NS providing sustained drug release (≈88.5% over 12 hours), surpassing both the pure drug and commercial formulations. Pharmacokinetic studies in rat's demonstrated significantly improved bioavailability, extended half-life, and increased mean residence time (MRT) for EZL-NS compared to the free drug. This confirms the potential of the nano sponge system to enhance therapeutic efficacy and reduce dosing frequency.

REFERENCES:

1. Okaiyeto, K., & Oguntibeju, O. (2021). African herbal medicines: Adverse effects and cytotoxic potentials with different therapeutic applications. *International Journal of Environmental Research and Public Health*, 18(5988). https://doi.org/10.3390/ijerph18115988
2. Kuruppu, A. I., Paranagama, P., & Goonasekara, C. L. (2019). Medicinal plants commonly used against cancer in traditional medicine formulae in Sri Lanka. *Saudi Pharmaceutical Journal*, 27, 565–573. Matowa, P. R., Gundidza, M., Gwanzura, L., & Nhachi, C. F. B. (2020). A survey of ethnomedicinal plants used to treat cancer by traditional medicine practitioners in Zimbabwe. *BMC Complementary Medicine and Therapies*, 20, 278.
3. Ahmadibeni, Y., Karim, K., & Boadi, W. (2017). Abstract 2180: Triphenylmethanol conjugates of leuprorelin as anti-cancer prodrugs. *Cancer Research*, 77(13 Supplement), 2180. Hashemi, S. R., & Davoodi, H. (2011). Herbal plants and their derivatives as growth and health promoters in animal nutrition. *Veterinary Research Communications*, 35, 169–180.
4. Kumar, G. P., & Khanum, F. (2012). Neuroprotective potential of phytochemicals. *Pharmacognosy Reviews*, 6, 81–90.
5. Alara, J. A., & Alara, O. R. (2019). Ethno-medicinal potentials and phytochemical properties of *Aloe vera*: A review. *Journal of Chemical Engineering, Industrial and Biotechnological Research*, 5, 57–73.
6. Crocetto, F., Di Zazzo, E., Buonerba, C., Aveta, A., Pandolfo, S. D., Barone, B., et al. (2021). Kaempferol, myricetin and fisetin in prostate and bladder cancer: A systematic review of the literature. *Nutrients*, 13(3750).
7. Iqbal, J., Abbasi, B. H., Mahmood, T., Kanwal, S., Ali, B., Shah, S. A., & Khalil, A. T. (2017). Plant-derived anticancer agents: A green anticancer approach. *Asian Pacific Journal of Tropical Biomedicine*, 7, 1129–1150.
8. Gori, J. L., Hsu, P., Maeder, M. L., Shen, S., Welstead, G. G., & Bumcrot, D. (2015). Delivery and specificity of CRISPR/Cas9 genome editing technologies for human gene therapy. *Human Gene Therapy*, 26, 443–451.
9. Chen, Y. H., Keiser, M. S., & Davidson, B. L. (2018). Viral vectors for gene transfer. *Current Protocols in Mouse Biology*, 8, e58.
10. Jan, R., & Chaudhry, G.-E. (2019). Understanding apoptosis and apoptotic pathways targeted cancer therapeutics. *Advanced Pharmaceutical Bulletin*, 9, 205–218.
11. Verma, A. K., Mandal, S., Tiwari, A., Monachesi, C., Catassi, G. N., Srivastava, A., et al. (2021). Current status and perspectives on the application of CRISPR/Cas9 gene-editing system to develop a low-gluten, non-transgenic wheat variety. *Foods*, 10(2351).
12. Singh, V., Khurana, A., Navik, U., Allawadhi, P., Bharani, K. K., & Weiskirchen, R. (2022). Apoptosis and pharmacological therapies for targeting thereof for cancer therapeutics. *Sci*, 4(15).
13. Sharifi, N., Salmaninejad, A., Ferdosi, S., Bajestani, A. N., Khaleghiyan, M., Estiar, M. A., et al. (2016). HER2 gene amplification in patients with prostate cancer: Evaluating a CISH-based method. *Oncology Letters*, 12, 4651–4658.
14. Rossini, A., Giussani, M., Ripamonti, F., Aiello, P., Regondi, V., Balsari, A., et al. (2020). Combined targeting of EGFR and HER2 against prostate cancer stem cells. *Cancer Biology & Therapy*, 21, 463–475.
15. Jiang, F., Liang, Y., Wei, W., Zou, C., Chen, G., Liu, Z., et al. (2020). Functional classification of prostate cancer-associated miRNAs through CRISPR/Cas9-mediated gene knockout. *Molecular Medicine Reports*, 22, 3777–3784.
16. Yao, Y., Zhou, Y., Liu, L., Xu, Y., Chen, Q., Wang, Y., et al. (2020). Nanoparticle-based drug delivery in cancer therapy and its role in overcoming drug resistance. *Frontiers in Molecular Biosciences*, 7, 193.
17. Desai, N., Momin, M., Khan, T., Gharat, S., Ningthoujam, R. S., & Omri, A. (2021). Metallic nanoparticles as drug delivery system for the

treatment of cancer. *Expert Opinion on Drug Delivery*, 18, 1261–1290.
18. Mount Sinai School of Medicine. (2019, August 27). Gold nanoparticles shown to be safe and effective treatment for prostate cancer. *ScienceDaily*. https://www.sciencedaily.com/releases/2019/08/190827123513.htm
19. Sechi, M., Sanna, V., & Pala, N. (2014). Targeted therapy using nanotechnology: Focus on cancer. *International Journal of Nanomedicine*, 9, 467–483.
20. Gregg, J. R., & Thompson, T. C. (2021). Considering the potential for gene-based therapy in prostate cancer. *Nature Reviews Urology*, 18, 170–184.
21. Balon, K., Sheriff, A., Jacków, J., & Łaczmański, Ł. (2022). Targeting cancer with CRISPR/Cas9-based therapy. *International Journal of Molecular Sciences*, 23, 573.
22. Amarachinta, P. R., Sharma, G., Samed, N., Chettupalli, A. K., Alle, M., & Kim, J. C. (2021). Central composite design for the development of carvedilol-loaded transdermal ethosomal hydrogel for extended and enhanced anti-hypertensive effect. *Journal of Nanobiotechnology*, 19, 1–5.
23. Chettupalli, A. K., Ananthula, M., Amarachinta, P. R., Bakshi, V., & Yata, V. K. (2021). Design, formulation, in-vitro and ex-vivo evaluation of atazanavir loaded cubosomal gel. *Biointerface Research in Applied Chemistry*, 11(4), 12037–12054.
24. Unnisa, A., Chettupalli, A. K., Al Hagbani, T., Khalid, M., Jandrajupalli, S. B., Chandolu, S., & Hussain, T. (2022). Development of dapagliflozin solid lipid nanoparticles as a novel carrier for oral delivery: Statistical design, optimization, in-vitro and in-vivo characterization, and evaluation. *Pharmaceuticals*, 15(5), 568.
25. Unnisa, A., Chettupalli, A. K., Hussain, T., & Kamal, M. A. (2022). Recent advances in epidermal growth factor receptor inhibitors (EGFRIs) and their role in the treatment of cancer: A review. *Anti-Cancer Agents in Medicinal Chemistry*, 22(20), 3370–3381.
26. Unnisa, A., Chettupalli, A. K., Alazragi, R. S., Alelwani, W., Bannunah, A. M., Barnawi, J., Amarachinta, P. R., Jandrajupalli, S. B., Elamine, B. A., Mohamed, O. A., & Hussain, T. (2023). Nanostructured lipid carriers to enhance the bioavailability and solubility of ranolazine: Statistical optimization and pharmacological evaluations. Pharmaceuticals, 16(8), 1151.
27. Chettupalli, A. K., Rao, P. A., Kuchukuntla, M., & Bakshi, V. (2020). Development and optimization of aripiprazole ODT by using Box–Behnken design. Research Journal of Pharmacy and Technology, 13(12), 6195–6201.
28. Avula, P. R., Chettupalli, A. K., Chauhan, V., & Jadi, R. K. (2023). Design, formulation, in-vitro and in-vivo pharmacokinetic evaluation of nicardipine-nanostructured lipid carrier for transdermal drug delivery system. Materials Today: Proceedings. Advance online publication. https://doi.org/10.1016/j.matpr.2023.07.012.
29. Prasad, R. R., Kumar, J. R., Vasudha, B. A., & Kumar, C. A. (2018). Formulation development and evaluation of allopurinol solid dispersions by solvent evaporation technique. International Journal of Applied Pharmaceutics, 10(4), 168–171.
30. Chettupalli, A. K., Amara, R. R., Amarachinta, P. R., Manda, R. M., Garige, B. S., & Yata, V. K. (2021). Formulation and evaluation of polyherbal liqui-solid compact for its anti-inflammatory effect. Biointerface Research in Applied Chemistry, 12, 3883–3899.
31. Chettupalli, A. K., Ajmera, S., Amarachinta, P. R., Manda, R. M., & Jadi, R. K. (2023). Quality by design approach for preparation, characterization, and statistical optimization of naproxen sodium-loaded ethosomes via transdermal route. Current Bioactive Compounds, 19(10), 79–98.
32. Unnisa, A., & Chettupalli, A. K. (2022). Promising role of phytochemicals in the prevention and treatment of cancer. Anti-Cancer Agents in Medicinal Chemistry, 22(20), 3382–3400.
33. Chettupalli, A. K., Ajmera, S., Kuchukuntla, M., Palanivel, V., & Katta, S. (2024). Design formulation of nanospanlastic novel carriers as a promising approach to enhanced bioavailability in intranasal drug delivery for sinusitis: Statistical optimization and in vitro and in vivo characterization. Current Nanomedicine, 14(3), 266–288.
34. Xu, H., Kita, Y., Bang, U., Gee, P., & Hotta, A. (2021). Optimized electroporation of CRISPR-Cas9/gRNA ribonucleoprotein complex for selection-free homologous recombination in human pluripotent stem cells. STAR Protocols, 2, 100965.
35. Rosenblum, D., Gutkin, A., Kedmi, R., Ramishetti, S., Veiga, N., Jacobi, A. M., et al. (2020). CRISPR-Cas9 genome editing using targeted lipid nanoparticles for cancer therapy. Science Advances, 6(47), eabc9450.
36. Ye, R., Pi, M., Cox, J. V., Nishimoto, S. K., & Quarles, L. D. (2017). CRISPR/Cas9 targeting of GPRC6A suppresses prostate cancer tumorigenesis in a human xenograft model. Journal of Experimental & Clinical Cancer Research, 36, 90.
37. Tsujino, T., Komura, K., Inamoto, T., & Azuma, H. (2021). CRISPR screen contributes to novel target discovery in prostate cancer. International Journal of Molecular Sciences, 22, 12777.
38. Friedman, A. D., Claypool, S. E., & Liu, R. (2013). The smart targeting of nanoparticles. Current Pharmaceutical Design, 19, 6315–6329.
39. Li, K., Zhan, W., Chen, Y., Jha, R. K., & Chen, X. (2019). Docetaxel and doxorubicin co-delivery by nanocarriers for synergistic treatment of prostate cancer. Frontiers in Pharmacology, 10, 1436.
40. Autio, K. A., Dreicer, R., Anderson, J., Garcia, J. A., Alva, A., Hart, L. L., et al. (2018). Safety and efficacy of BIND-014, a docetaxel nanoparticle targeting prostate-specific membrane antigen for patients with metastatic castration-resistant prostate cancer: A phase 2 clinical trial. JAMA Oncology, 4(9), 1344–1351.
41. Johannsen, M., Thiesen, B., Wust, P., & Jordan, A. (2010). Magnetic nanoparticle hyperthermia for prostate cancer. International Journal of Hyperthermia, 26(8), 790–795.

42. He, M.-H., Chen, L., Zheng, T., Tu, Y., He, Q., Fu, H.-L., et al. (2018). Potential applications of nanotechnology in urological cancer. Frontiers in Pharmacology, 9, 745.
43. Yap, T. A., Smith, A. D., Ferraldeschi, R., Al-Lazikani, B., Workman, P., & De Bono, J. S. (2016). Drug discovery in advanced prostate cancer: Translating biology into therapy. Nature Reviews Drug Discovery, 15, 699–718.
44. Tüfekci, K. U., Öner, M. G., Meuwissen, R. L. J., & Genç, Ş. (2013). The role of microRNAs in human diseases. In miRNomics: MicroRNA Biology and Computational Analysis (pp. 33–50). Humana Press.
45. Johnson, T. M. (2017). Perspective on precision medicine in oncology. Pharmacotherapy: The Journal of Human Pharmacology and Drug Therapy, 37(8), 988–989.
46. Aiassa, V., Garnero, C., Longhi, M. R., & Zoppi, A. (2021). Cyclodextrin multicomponent complexes: Pharmaceutical applications. Pharmaceutics, 13(7), 1099.
47. Mane, P. T., Wakure, B. S., & Wakte, P. S. (2021). Cyclodextrin-based nanosponges: A multidimensional drug delivery system and its biomedical applications. Current Drug Delivery, 18(10), 1467–1493.
48. Sherje, A. P., Dravyakar, B. R., Kadam, D., & Jadhav, M. (2017). Cyclodextrin-based nanosponges: A critical review. Carbohydrate Polymers, 173, 37–49.
49. Iravani, S., & Varma, R. S. (2022). Nanosponges for water treatment: Progress and challenges. Applied Sciences, 12(9), 4182.
50. Lembo, V., Folini, D., Wild, M., & Lionello, P. (2019). Inter-hemispheric differences in energy budgets and cross-equatorial transport anomalies during the 20th century. Climate Dynamics, 53(1), 115–135.
51. Almutairy, B. K., Alshetaili, A., Alali, A. S., Ahmed, M. M., Anwer, M. K., & Aboudzadeh, M. A. (2021). Design of olmesartan medoxomil-loaded NSs for hypertension and lung cancer treatments. Polymers, 13(14), 2272.